



# Prediction of depth-averaged velocity in an open channel flow

Jnana Ranjan Khuntia<sup>1</sup> · Kamalini Devi<sup>1</sup> · Kishanjit Kumar Khatua<sup>1</sup>

Received: 19 November 2017 / Accepted: 11 September 2018 / Published online: 22 September 2018  
© The Author(s) 2018

## Abstract

This paper presents a new methodology to predict the depth-averaged velocity along the lateral direction in an open channel flow. The novelty of this work is to determine the point velocity and estimate the discharge capacity by knowing the geometrical parameters at a section of an open channel flow. Experimental investigations have been undertaken in trapezoidal and rectangular channels to observe the variation of local velocities along both the vertical and transverse directions at testing sections. For different geometry, hydraulic and roughness conditions, the measurements are taken for several flow conditions. Multi-variable regression analysis has been adopted to develop five models to predict the point velocities in terms of non-dimensional geometric and flow parameters at any desired location. The present method is favourably compared with the analytical method of Shiono and Knight with reasonable accuracy. The performance of mathematical model is also validated with two natural river data sets. Further, statistical error analysis is carried out to know the degree of accuracy of the present models.

**Keywords** Open channel flow · Velocity profiles · Regression analysis · Depth-averaged velocity · Error analysis

## List of symbols

$b$	Total width and top width of rectangular and trapezoidal channel, respectively	$\rho$	Water density
$b/2$	Half width of the channel	$g$	Acceleration due to gravity
$H$	Flow depth	$u, v, w$	Components of velocity along $x, y, z$ directions, respectively
$n$	Manning's roughness coefficient	$u', v', w'$	Components of turbulence intensity along $x, y, z$ directions, respectively
$z$	Vertical coordinate above the bed along depth of flow	$\bar{u}, \bar{v}, \bar{w}$	Time-averaged mean velocity along $x, y, z$ directions, respectively
$y$	Lateral coordinate along the width of the channel	$f$	Darcy–Weisbach friction factor
$U$	Point/local velocity	$\lambda$	Dimensionless eddy viscosity
$U_{\text{mean}}$	Mean velocity	$\Gamma$	Secondary flow parameter
$S_0$	Bed slope/longitudinal slope	$s$	Side slope
$Q$	Discharge of the channel	$R^2$	Coefficient of deterministic
$A$	Wetted area of cross section	MAPE	Mean absolute percentage error
$P$	Wetted perimeter of the channel	RMSE	Root-mean-square error
$R = A/P$	Hydraulic radius of channel	FCF	Flood channel facility
$\tau$	Boundary shear stress		

✉ Jnana Ranjan Khuntia  
jnanaranjan444@gmail.com

Kamalini Devi  
kamalinidevi1@gmail.com

Kishanjit Kumar Khatua  
kkkhatua@yahoo.com

<sup>1</sup> Civil Engineering Department, National Institute of Technology, Rourkela, India

## Introduction

Rivers have been used as a source of water for procuring food, transport, navigation and as a source to generate hydro-power to operate machinery. Generally, the water in a river is restricted to a channel, assembled with stream bed and side banks. Understanding the flow velocity of these rivers is most crucial for river engineers for a broad range of application in different exercises such as the meticulous study

of water quantity and quality. Further, vertical and lateral velocity distributions are the fundamental understanding of the state of flow in channels, as required for flow modelling, extremity spill management and for different technical aspects related to living organisms and human beings. Generally, the velocity in a cross section differs from point to point, due to the effects of water surface and shear stress at the bed. As the velocity distribution in an open channel is complex, modelling the velocity is not an easy task (Maghrebi and Givvehchi 2009). Flow prediction of natural rivers and urban channels are accurately evaluated from the vertical and lateral velocity distributions in association with depth-averaged velocity for several geometric conditions. Hydraulic engineers are always searching for suitable methods of calculating mean discharge in the channels having different shapes and sizes with minimal need of substantial measurement (Jan et al. 2009).

Sarma et al. (1983) studied velocity distributions in a smooth rectangular channel by dividing the channel into four regions for different ranges of hydraulic parameters. Steffler et al. (1985) measured mean velocity as well as turbulence for uniform flow in a smooth rectangular channel for three different aspect ratios such as 5.08, 7.83 and 12.3. They studied the logarithmic law of velocity distribution in the respective channels. Tominaga et al. (1989) studied the secondary currents and also modified the turbulence anisotropy which is affected by the boundary conditions of the bed, the side walls, the free surface as well as the aspect ratio and geometry of the channels. Blumberg et al. (1992) conducted experiments in both smooth and rough open channels and incorporated second-moment turbulence closure model to simulate turbulent flows with various geophysical and engineering boundary layers. Nezu et al. (1997) conducted experiments to measure the turbulence successfully over a smooth bed with non-uniform and unsteady flow. They utilised the two-component laser Doppler anemometer (LDA) to measure the two components of velocity. Shiono and Feng (2003) presented the turbulence measurements of velocity and tracer concentration in rectangular and compound channels using a combination of Laser Doppler anemometer (LDA) and laser induced fluorescence (LIF). Liao and Knight (2007) derived three analytical models which were suitable for hand calculation to find out the stage-discharge relationship in simple channels as well as in symmetric and asymmetric compound channels. Zarrati et al. (2008) modelled semi-analytical equations for distribution of shear stress in straight open channels with rectangular, trapezoidal, and compound cross-sectional areas. Ansari et al. (2011) exhibited the utilization of computational fluid dynamics (CFD) to estimate the bed shear and wall shear stresses in trapezoidal channels. Specifically for low aspect ratio channels, the variety of inclination angle and aspect ratio conveyed significant changes to the distribution of the shear stress at the boundaries as well

as in the flow structures as already shown by De Cacqueray et al. (2009). Jesson et al. (2012) simulated the open channel flow over a heterogeneous roughened bed and also analysed it both physically and numerically. The velocity field was mapped at four distinctive cross sections by utilizing an Acoustic Doppler Velocimeter (ADV) and the boundary shear stress is obtained by using the Preston tube technique. Yang et al. (2012) proposed a depth-averaged equation of flow by analysing the forces acting on the natural water body and utilizing the Newton's second law. Khuntia et al. (2016) investigated experimentally the variation of global and local friction factor based on the measurement of depth-averaged velocity and boundary shear stress over the cross section in channels of different geometries.

Shiono and Knight (1990) simplified the momentum equation to estimate the lateral depth-averaged velocity and boundary shear distribution, and their method is popularly known as Shiono and Knight Method (SKM). The SKM method offers an improved analytical solution to predict the flow parameters in an open channel flow; however, it depends on the three calibrating parameters i.e.  $f$ ,  $\lambda$ , and  $\Gamma$  before its application.

So, considering the importance of the velocity distribution for the estimation of a number of hydraulic parameters, it is necessary to derive a common, precise and user-friendly method to evaluate the local velocity at any desired point. This local velocity at every point helps to estimate the distribution of depth-averaged velocity and overall flow in a channel. The objective of this paper is to develop expressions to predict local velocities at any desired location of homogeneous roughness channels, which in turn help to estimate the flow distribution and stage-discharge relationships.

## Experimental setup and procedure

Two sets of experiments were carried out in glass-walled tilted flumes of 22 m long, 0.34 m wide and 0.113 m deep with bed slope of 0.0015 and 15 m long, 0.33 m wide, 0.11 m deep with bed slope 0.001 at the fluid mechanics and hydraulics laboratory, National Institute of Technology, Rourkela (NITR). The cross-sectional details of experimental channels are shown in Fig. 1. The boundaries of experimental channels were kept smooth for those two cases in the first cycle of the experiment. For smooth bed, the materials used were trowel finished cement concrete surface ( $n = 0.01$ ). Then the bed of the trapezoidal channel changed to the rough boundary by using small gravel. For rough bed, small gravels of  $d_{50} = 20$  mm size having Manning's  $n$  value 0.02 has been used. The test section was considered 10 m away from the bell-mouthed entrance towards the downstream. A point gauge with least count 0.01 m is used along the centreline of the flume for measuring the depth of water.

The fabricated experimental channels of NITR are shown in Fig. 2, and details of geometric and hydraulic parameters used for experimentations are given in Table 1. All depths were measured with respect to the bottom of the flume for smooth cases. For rough case, flow depths were measured from a reference line located between the bottom of the bed and top surface of the roughened materials. The discharges were measured using volumetric tank at the downstream end of the flume. A vertical piezometer with water table indicator of least count 0.1 cm is fitted to the volumetric tank which helps to measure the constant rise of water in it. For this purpose, the passing way of water from the volumetric tank to underground sump has been closed by a valve. The time of rise in water level in the piezometer is recorded by a

stopwatch. The volume of water is the product of volumetric tank area and height of 1 cm water rise in the piezometer. Finally, the discharge is calculated by dividing the volume of water to the time required (in seconds) in rising 1 cm of water. The discharge is thus computed for every experimental run through time rise method.

The velocities were measured by a SonTek Micro 16-MHz Acoustic Doppler Velocimeter (ADV). The sampling rate is 50 Hz (the maximum). Sampling volume of ADV is located approximately 5 cm below the down looking probe and was set to be minimum of 0.09 cm<sup>3</sup>. The 5 cm distance between the probe and sampling volume minimizes the flow interference. A total of 2, 97,000 data points were recorded (at 50 Hz) for a total recording length of 99 min for rectangular

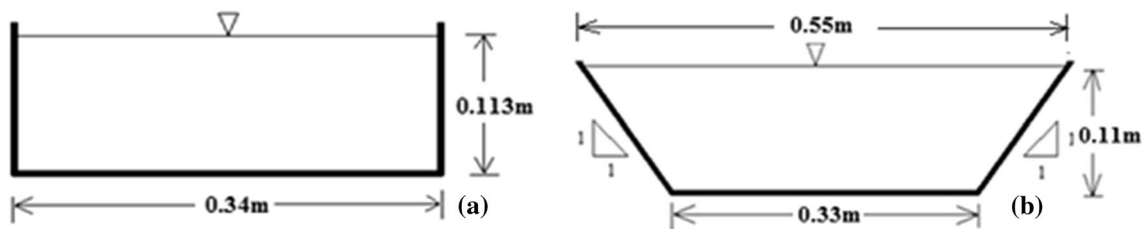


Fig. 1 Cross section of experimental channels of NITR a rectangular, b trapezoidal

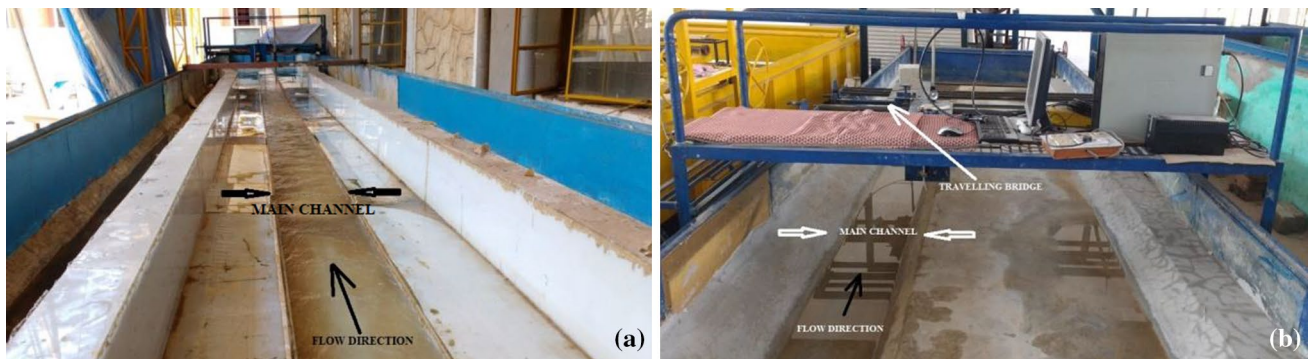


Fig. 2 Fabricated experimental channels of NITR a rectangular, b trapezoidal (Test section is only main channel)

Table 1 Details of geometric and hydraulic parameters of the experimental setup

Series name	Shape	Surface condition	Bed width $B(m)$	Flow depth $H(m)$	Roughness value ( $n$ )	Bed slope $S_0$	Discharge $Q (m^3/s)$
NITR1	Rectangular	Smooth	0.34	0.076–0.107	0.01	0.0015	0.012–0.020
NITR2	Trapezoidal	Smooth	0.33	0.08–0.11	0.011	0.001	0.016–0.026
NITR3	Trapezoidal	Rough	0.33	0.07–0.09	0.02	0.001	0.006–0.01
FCF	Trapezoidal	Smooth	1.5	0.049–0.149	0.01	0.00103	0.029–0.202
Tominaga et al. (1989) S1	Rectangular	Smooth	0.4	0.05–0.199	0.01	0.000937	0.008–0.015
Tominaga et al. (1989) S2	Trapezoidal	Smooth	0.152	0.071	0.01	0.000594	0.0062
Tominaga et al. (1989) S3	Trapezoidal	Smooth	0.2	0.091	0.01	0.000594	0.010
Tominaga et al. (1989) S4	Trapezoidal	Smooth	0.248	0.11	0.01	0.000594	0.011

channel and 3, 87,000 data points were recorded (at 50 Hz) for a total recording length of 129 min for trapezoidal channel. Correlation has been used to monitor data quality during collection and to edit data in post-processing. Ideally, correlation should be between 70 and 100%. Signal-to-noise ratio (i.e. SNR) is a measure that compares the level of a desired signal to the level of background noise. It can be accessed as signal amplitude in internal logarithmic units called signal-to-noise ratio (SNR) in dB. The range of SNR (signal-to-noise ratio) value should be higher than 20 dB for 16-MHz micro-ADV. So, it was necessary to maintain the value of SNR for each data points reordered using micro-ADV.

Other two data sets from Flood Channel Facility (FCF) and Tominaga et al. (1989) have been considered for present analysis. The UK Flood Channel Facility is a large-scale national facility for undertaking experimental investigations of in-bank and overbank flows in rivers. The FCF (Series A) in-bank dataset was used for this present analysis. The FCF was 56 m long and 10 m wide with a usable length of 45 m. The longitudinal bed slope was  $1.027 \times 10^3$ . Further, two experimental data sets of Tominaga et al. (1989) were used in this study. The experiments were conducted in a tilting

flume with 12.5 m length but having different cross-sectional geometries and longitudinal slopes as given in Table 1.

### Model development

Depth-averaged velocity is an important output for every experimental study as well as in analytical study. But the procedure of determination may be different. So, this paper tries to derive five expressions in five desired vertical locations, i.e. at  $0.2H$ ,  $0.4H$ ,  $0.6H$ ,  $0.8H$ , and  $0.95H$ , where  $H$  is the total flow depth. In turn, it will help to find out the depth-averaged velocity at various vertical interfaces. The depth-averaged velocity at each interface can be found out by integrating the velocities over the flow depth found from the derived expressions at five vertical positions. Then the distribution of depth-averaged velocity along the lateral section will be the line joining of individual depth-averaged velocities at each vertical interface. Variation of dimensionless vertical velocity distribution is shown in Fig. 3, and lateral variations of dimensionless velocities at five vertical positions are shown in Figs. 4, 5, 6, 7 and 8, respectively.

**Fig. 3** Variation of dimensionless vertical velocity distribution

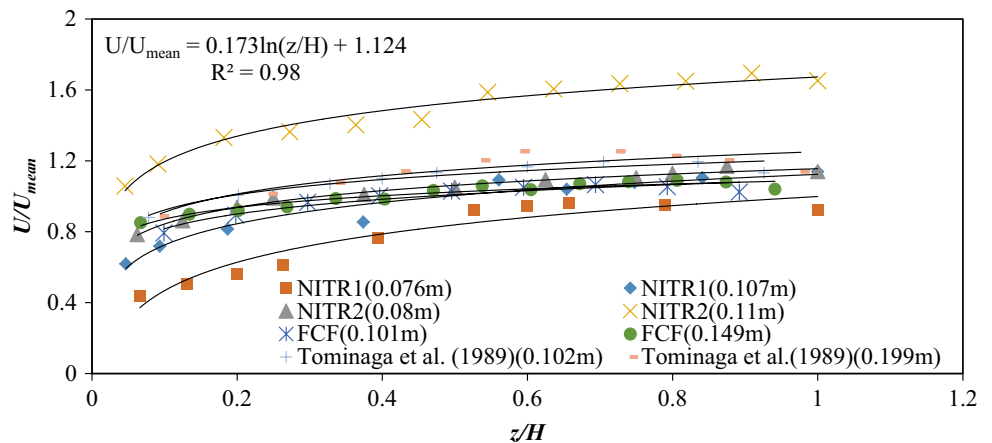


**Fig. 4** Lateral variation of dimensionless velocities at a position of  $0.2H$

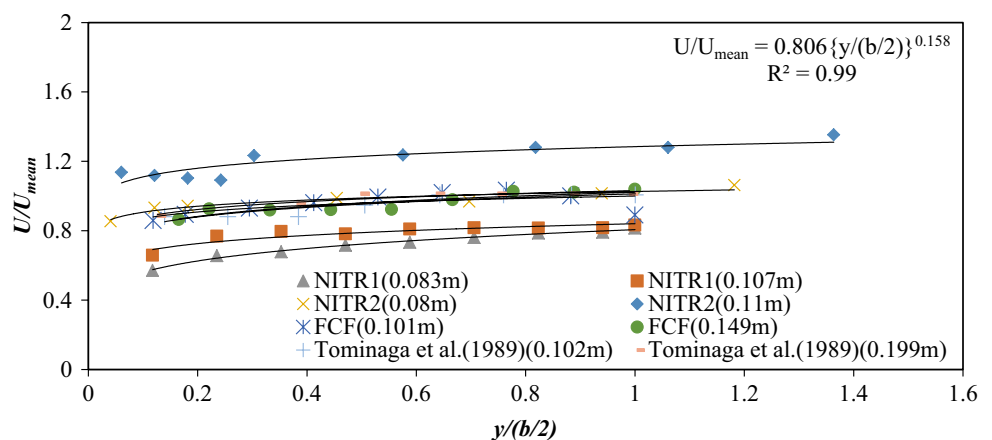


**Fig. 5** Lateral variation of dimensionless velocities at a position of  $0.4H$

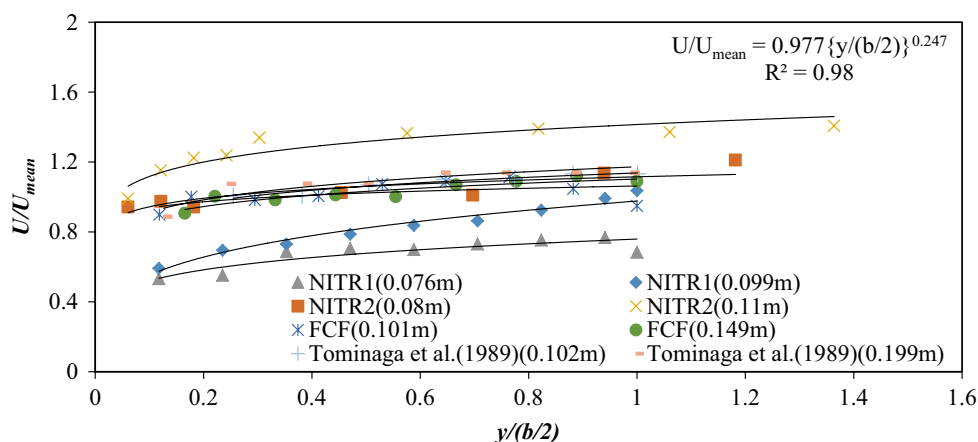


**Fig. 6** Lateral variation of dimensionless velocities at a position of  $0.6H$

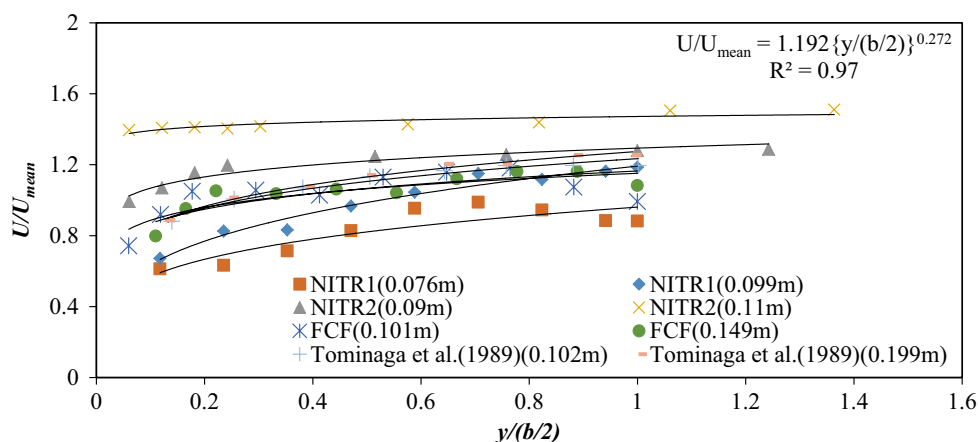
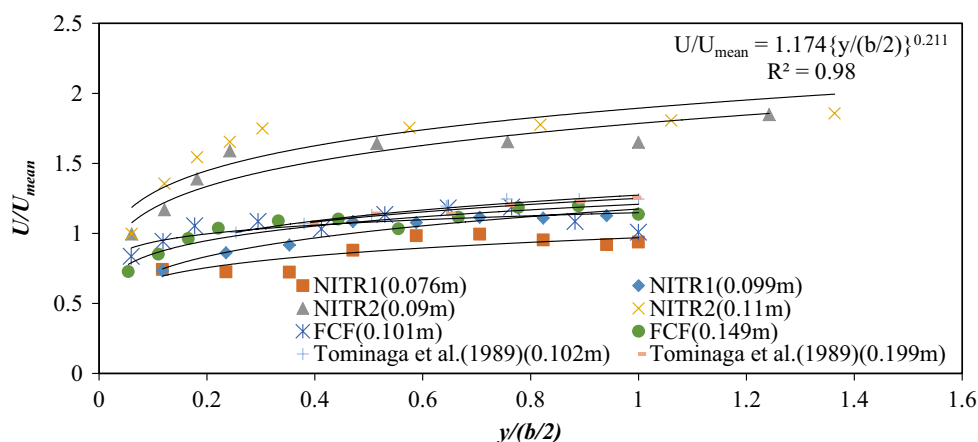


**Fig. 7** Lateral variation of dimensionless velocities at a position of  $0.8H$



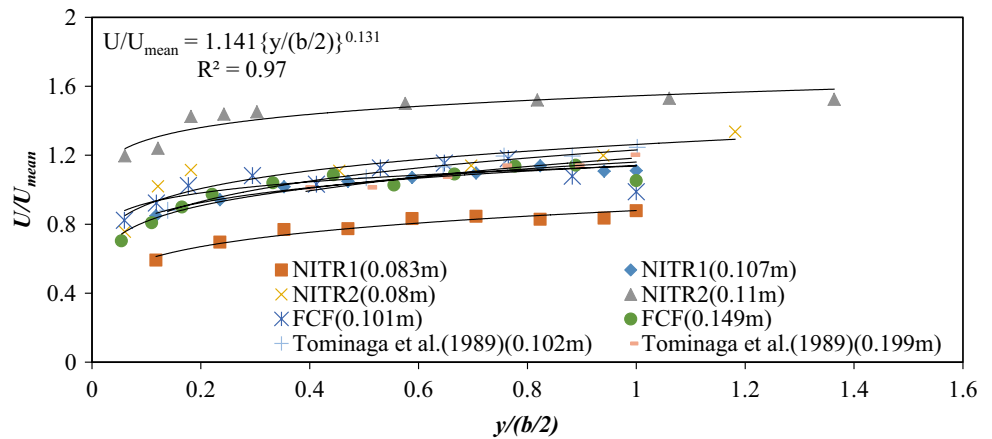
**Multi-variable regression analysis**

In this present study, a number of possible single regression models considering different one to one relationships (e.g. exponential, power, linear or logarithmic) between the dependent parameter and independent parameters were tested. The selection of best regression models was achieved

based on the highest coefficient of determination ( $R^2$ ) values. Two preferred input independent variables have been used for this study since these variables are found to control the shear distribution. Multi-variable regression analysis compiles these two independent variables to model up the dependent variable. Finally, through multi-variable regression analysis, five models have been derived with high coefficient of determinations for five vertical positions.



**Fig. 8** Lateral variation of dimensionless velocities at a position of 0.95H



Here, two independent parameters like lateral dimension ( $y$ ) and vertical dimension ( $z$ ) were made dimensionless as  $\left(\frac{y}{b/2}\right)$  and  $\left(\frac{z}{H}\right)$ , respectively, for estimating the dimensionless local velocities  $\left(\frac{U}{U_{mean}}\right)$  at desired locations, where  $y$  and  $z$  are lateral coordinate along the width of the channel and vertical coordinate above the bed along depth of flow, respectively. The independent variables were made dimensionless by dividing the cross-sectional geometric dimensions such as half bottom width ( $b/2$ ) and hydraulic dimensions such as flow depths ( $H$ ). Experimental point velocity data sets were arranged, and then the vertical and lateral velocity distributions along the cross section of the channel have been drawn at desired locations (i.e.  $0.2H$ ,  $0.4H$ ,  $0.6H$ ,  $0.8H$ , and  $0.95H$ ). Then for vertical velocity profile, the best relationships obtained are logarithmic in nature for every position along the lateral distance for all flow depths. Among all the vertical velocity profiles, the best relationship with high regression coefficient (i.e.  $R^2 \approx 0.98$ ) has been taken for regression analysis (Fig. 3). For lateral velocity profiles, five different power functional equations were taken with maximum  $R^2$  (i.e.  $R^2 \approx 0.99, 0.98, 0.97, 0.98$  and  $0.97$  for  $0.2H, 0.4H, 0.6H, 0.8H$  and  $0.95H$ , respectively) as shown in Figs. 4, 5, 6, 7 and 8. Finally, five multi-variable regression models have been developed for finding out the lateral velocity profiles at  $0.2H, 0.4H, 0.6H, 0.8H$  and  $0.95H$  with given values of  $\left(\frac{y}{b/2}\right)$  and  $\left(\frac{z}{H}\right)$  and depicted in Eqs. 1 to 5 with large  $R^2$  values.

$$\left(\frac{U}{U_{mean}}\right)_{0.2H} = 0.44 - 0.02 \ln\left(\frac{z}{H}\right) + 0.55 \left(\frac{y}{b/2}\right)^{0.158} \tag{1}$$

$$\left(\frac{U}{U_{mean}}\right)_{0.4H} = 1.01 + 0.38 \ln\left(\frac{z}{H}\right) + 0.46 \left(\frac{y}{b/2}\right)^{0.247} \tag{2}$$

$$\left(\frac{U}{U_{mean}}\right)_{0.6H} = 0.56 - 0.21 \ln\left(\frac{z}{H}\right) + 0.48 \left(\frac{y}{b/2}\right)^{0.272} \tag{3}$$

$$\left(\frac{U}{U_{mean}}\right)_{0.8H} = 0.50 - 0.04 \ln\left(\frac{z}{H}\right) + 0.68 \left(\frac{y}{b/2}\right)^{0.211} \tag{4}$$

$$\left(\frac{U}{U_{mean}}\right)_{0.95H} = 1.26 + 1.41 \ln\left(\frac{z}{H}\right) + 0.57 \left(\frac{y}{b/2}\right)^{0.131} \tag{5}$$

Equations 1 to 5 depend on the non-dimensional parameters  $z/H$  and  $y/(b/2)$ . So the coefficients for these parameters are greatly influencing the model results. However, it is true that  $z/H$  term of these equations can be replaced by 0.2, 0.4, 0.6, 0.8 and 0.95, respectively. But it cannot be removed absolutely. This model provides the ratio of  $\left(\frac{U}{U_{mean}}\right)$  at desired locations, where  $U$  is local or point velocity and  $U_{mean}$  is mean velocity of a flow depth. Where  $U_{mean}$  will be calculated by using convenient Manning's or Chezy's equation with given geometric conditions. Then multiplying the mean velocity ( $U_{mean}$ ) with  $\left(\frac{U}{U_{mean}}\right)$ , the local velocity or point velocity ( $U$ ) can be obtained at desired locations. The local velocity ( $U$ ) can further be utilised to find out the

depth-averaged velocity ( $U_d$ ) at any vertical position for all given depths of NITR channel, FCF channel and Tominaga et al. (1989) channels. The equations from 1 to 5 have been developed using NITR series data (i.e. NITR1 and NITR2) as well as selected data of FCF and Tominaga et al. (1989). Then, it has been validated with the experimental data sets of NITR3 series, FCF and Tominaga et al. 1989. Moreover, these equations are applied to natural river data sets which show the efficacy of the models. The  $U_d$  is calculated by integrating local point stream-wise velocities ( $U$ ) over a flow depth  $H$  using Eq. 6.

$$U_d = \frac{1}{H} \int_0^H U dz. \tag{6}$$

### Application of Shiono and Knight model (SKM)

Shiono and Knight integrated the Navier–Stokes equation that is the momentum equation over the flow depth  $H$ , mainly to find out the lateral depth-averaged velocity distribution. The method of solving this equation is known as Shiono and Knight method.

So, for steady uniform flows, the Reynolds-Average Navier–Stokes equation (RANS) is simplified as (Devi and Khatua 2016)

$$v \frac{\partial^2 \bar{u}}{\partial y^2} + v \frac{\partial^2 \bar{u}}{\partial z^2} - \frac{\partial \bar{u}'v'}{\partial y} - \frac{\partial \bar{u}'w'}{\partial z} + g \left\{ \frac{\partial h}{\partial x} - S_0 \right\} = \frac{\partial \bar{u}\bar{v}}{\partial y} + \frac{\partial \bar{u}\bar{w}}{\partial z} \tag{7}$$

This generalized equation for obtaining the turbulent flow structure is applicable in different flow conditions. The RANS equation in longitudinal flow direction ( $X$  direction) can be written as

$$\rho \left[ \frac{\partial \bar{u}\bar{v}}{\partial y} + \frac{\partial \bar{u}\bar{w}}{\partial z} \right] = \rho g S_0 + \frac{\partial}{\partial y} \left( -\rho \overline{u'v'} \right) + \frac{\partial}{\partial z} \left( -\rho \overline{u'w'} \right) \tag{8}$$

where  $u'$ ,  $v'$  and  $w'$  are the fluctuation of the velocity components along  $x$  (along the flow),  $y$  (lateral to the bed of flume) and  $z$  (vertical to the bed of flume) directions, respectively,  $\bar{u}$ ,  $\bar{v}$  and  $\bar{w}$  are the components of the mean velocity along  $x$  (along the flow),  $y$  (lateral to the bed of flume) and  $z$  (vertical to the bed of flume) directions, respectively,  $\rho$ =density of the water,  $S_0$ =longitudinal bed slope,  $g$ =acceleration due to gravity.

The simplified form of Eq. 8 is given as

$$\rho \frac{\partial H(\bar{u}\bar{v})_d}{\partial y} = \rho H g S_0 + \frac{\partial}{\partial y} \left( \rho \lambda H^2 \left( \frac{f}{8} \right)^{\frac{1}{2}} U \frac{\partial U}{\partial y} \right) - \frac{f}{8} \rho U^2 \sqrt{1 + \frac{1}{s^2}} \tag{9}$$

This is the simplified final form of SKM. Here the first term of the left-hand side is because of secondary current ( $\Gamma$ ). The first term of the right-hand side is the gravitational term, the second term is the Reynolds shear stress and the third term is because of the bed shear stress. So, the solution of Eq. 9 relies on three calibrating coefficients  $f$ ,  $\lambda$ , and  $\Gamma$ , identified with local bed friction factor, eddy viscosity, and the secondary flow term, respectively. Shiono and Knight (1990) proposed analytically by taking appropriate values from their own particular experimental outcomes and presumed that the secondary flow varies linearly in lateral direction; therefore, they replaced the left-hand side term in the equation by a constant,  $\Gamma$ .

$$\frac{\partial}{\partial y} [H(\rho UV)_d] = \Gamma \tag{10}$$

Considering Eq. 10, the general solution for  $U_d$  in constant flow depth domain (bed region) and in variable flow depth domain (side slope region) is extracted from Eq. 9 as specified below

$$U_d(y) = [A_1 e^{\gamma y} + A_2 e^{-\gamma y} + k]^{1/2} \tag{11}$$

where  $\gamma = \left( \frac{f}{8} \right)^{\frac{1}{4}} \left( \frac{2}{\lambda} \right)^{\frac{1}{2}} \left( \frac{1}{H} \right)$  and  $k = \frac{C}{B} = K(1 - \beta)$ ; and  $K = \frac{8gS_0H}{f}$ ,  $\beta = \frac{\Gamma}{\rho g S_0 H}$  and for a variable flow depth domain (i.e. linear side slope 1:s)

$$U_d(y) = [A_3 \xi^\alpha + A_4 \xi^{-(\alpha+1)} + \omega \xi + \eta]^{1/2} \tag{12}$$

where

$$\alpha = \frac{1}{2} + \frac{1}{2} \sqrt{1 + \frac{s \sqrt{8f} \sqrt{1 + s^2}}{\lambda}}; \tag{13}$$

$$\omega = \frac{g S_0}{\frac{\sqrt{1+s^2}}{s} \left( \frac{f}{8} \right) - \frac{\lambda \sqrt{f/8}}{s^2}}; \eta = \frac{-\Gamma}{\rho \left( \frac{f}{8} \right) \sqrt{1 + \frac{1}{s^2}}};$$

$$\xi = H + \frac{y+b}{s} \text{ (for positive } y) \quad \xi = H - \frac{y-b}{s} \text{ (for negative } y) \tag{14}$$

Before evaluation of  $U_d$  in the lateral direction, three important calibration coefficients  $f$ ,  $\lambda$ ,  $\Gamma$  need to be calibrated. Analytically, the SKM can be executed effectively if the channel is partitioned into reasonable panels where the calibrating coefficients are portrayed enough with fitting boundary conditions.

The predicted depth-averaged velocity distributions found from Eqs. 1–5 is compared with their experimental values as well as with SKM and demonstrated in a single graph for some typical flow depths. Figures 9, 10 and 11 show these comparisons for NITR series. The photograph

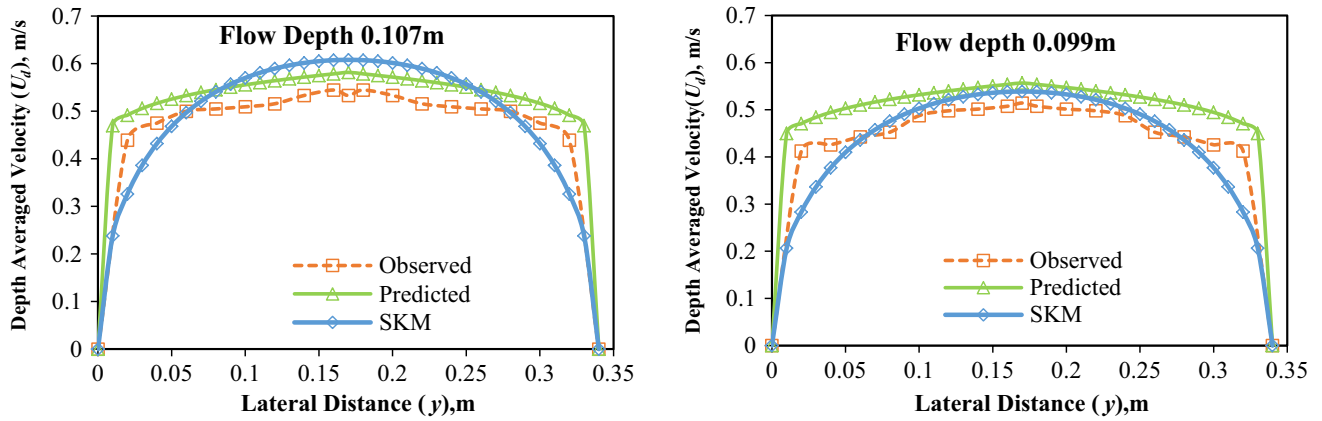


Fig. 9 Depth-averaged velocity of NITR1 series

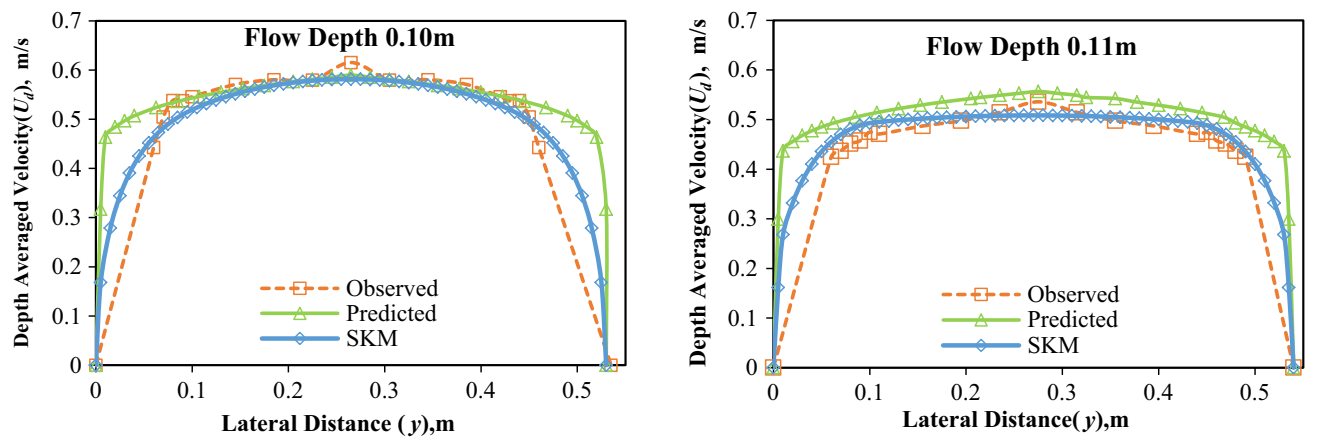


Fig. 10 Depth-averaged velocity of NITR2 series

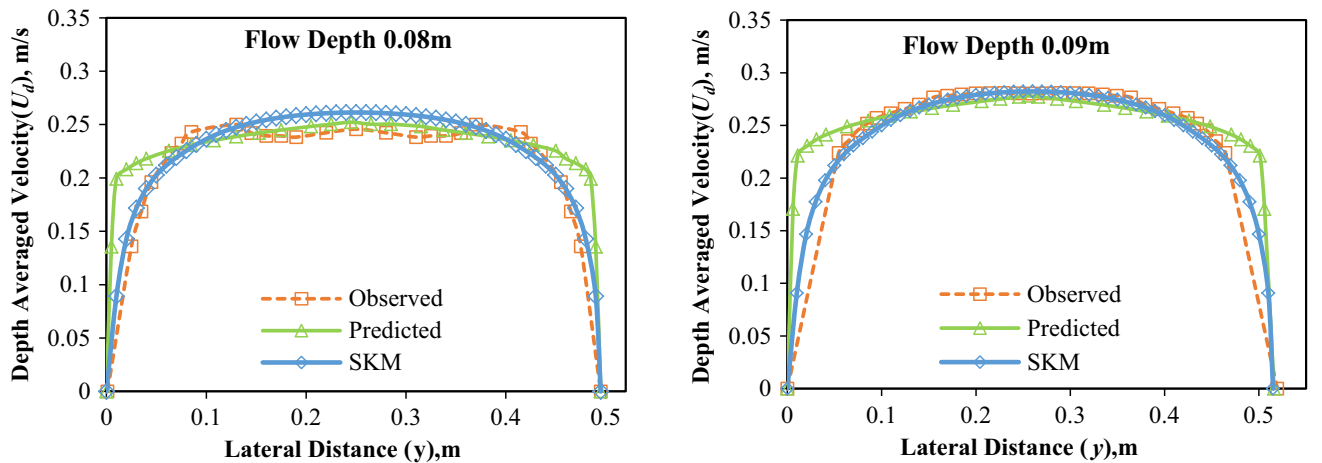
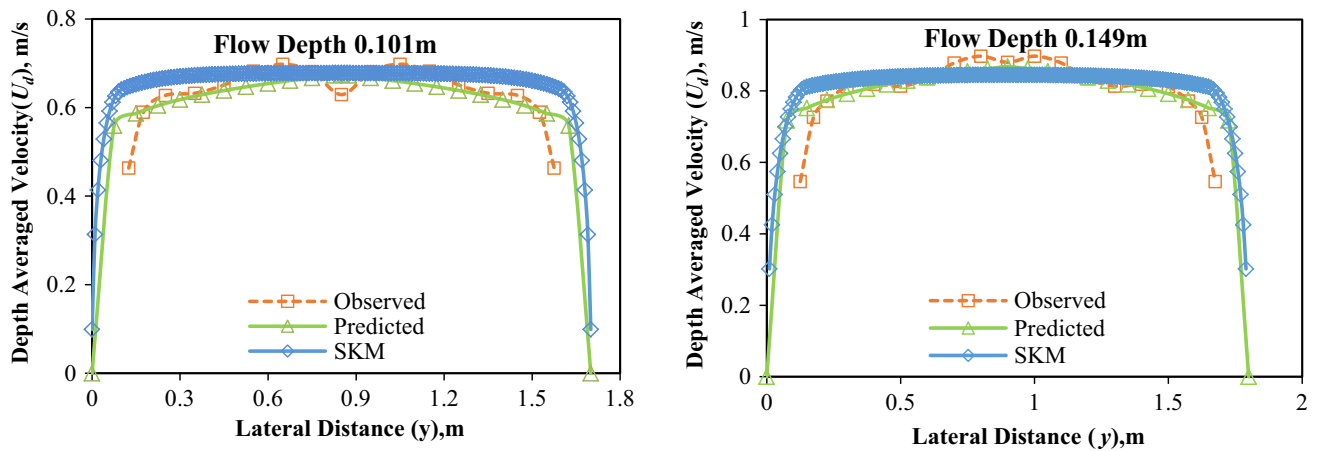


Fig. 11 Depth-averaged velocity of NITR3 series



**Fig. 12** Experimental channel of SERC facility at Wallingford (FCF), UK



**Fig. 13** Depth-averaged velocity of FCF,UK channel series

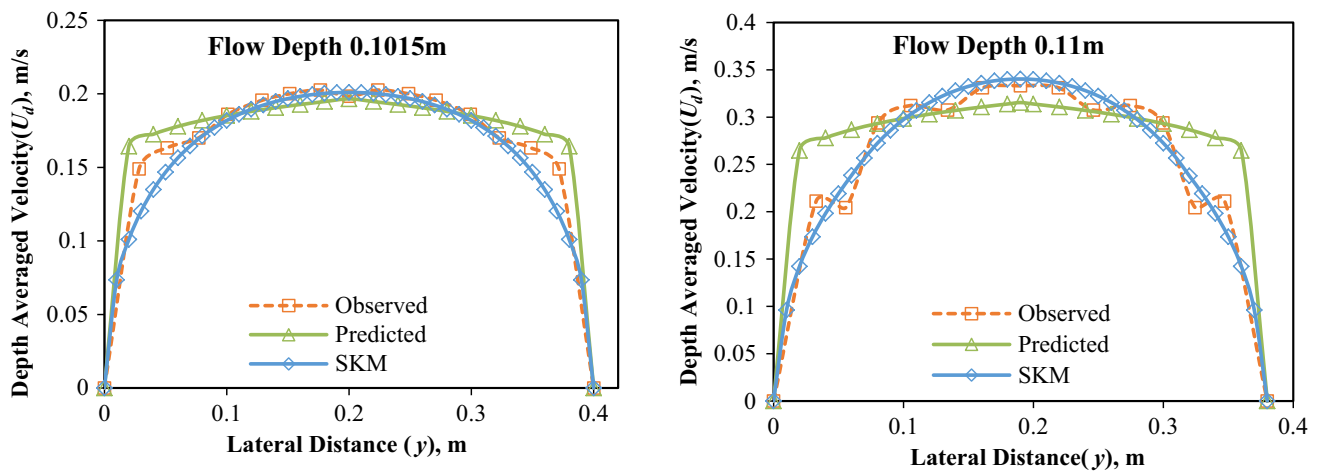


**Fig. 14** Depth-averaged velocity of Tominaga et al. (1989) series

of the experimental channel of SERC Facility at Wallingford (FCF), UK shown in Fig. 12. Figures 13 and 14, presents the depth-averaged velocity distribution for FCF and Tominaga et al. (1989) datasets, respectively.

### Results and discussions

The lateral velocity profiles at different planes are found to be power in function, and vertical velocity profiles are found to be logarithmic in nature. The SKM model is found to provide satisfactory velocity profile results; however, it fails to predict velocities at the junction between the constant flow depth domain and variable flow depth domain. Equations 1–5, based on multi-variable regression analysis, are found to provide good results for predicting velocity profiles in both lateral and vertical directions. The values of regression coefficient ( $R^2$ ) for 0.2H, 0.4H, 0.6H, 0.8H and 0.95H profiles were found between 0.85 and 0.97. For applying Eqs. 1–5, there are certain ranges of non-dimensional independent and dependent parameters. The ranges of the parameters are: for  $U/U_{mean}=0.4$  to 1.87, for  $z/H=0.2, 0.4, 0.6, 0.8$  and 0.95 and for  $y/(b/2)=0$  to 1.

Further, statistical error analysis has been performed to evaluate the strength of the present work. Two error analyses were done such as the mean absolute percentage error (MAPE), and root-mean-square error (RMSE). MAPE and RMSE have been computed for each respective value by using the formulae given in Eqs. 15 and 16, respectively.

$$MAPE = \frac{1}{n} \sum \left| \frac{V_{observed} - V_{predicted}}{V_{observed}} \right| \times 100 \quad (15)$$

$$RMSE = \sqrt{\frac{1}{n} \sum (V_{observed} - V_{predicted})^2} \quad (16)$$

**Table 2** RMSE results of depth-averaged velocity distribution by different models

Channel type	RMSE	
	Present model	SKM
NITR1 ( $H=0.11$ m)	0.043	0.066
NITR1 ( $H=0.10$ m)	0.056	0.074
NITR2 ( $H=0.10$ m)	0.012	0.033
NITR2 ( $H=0.11$ m)	0.064	0.065
NITR3 ( $H=0.08$ m)	0.014	0.015
NITR3 ( $H=0.09$ m)	0.007	0.008
FCF ( $H=0.10$ m)	0.045	0.070
FCF ( $H=0.15$ m)	0.066	0.093
Tominaga et al. (1989) S1 ( $H=0.10$ m)	0.056	0.074
Tominaga et al. (1989) S4 ( $H=0.11$ m)	0.041	0.018

where  $V_{predicted}$  and  $V_{observed}$  are the predicted value and observed value of velocity, respectively.

The MAPE values has been computed for the data sets of large channel facility of FCF and data of Tominaga et al. (1989) shown in Fig. 15. RMSE values found for the present models and SKM have also been verified through the data sets of FCF, Tominaga et al. (1989) and rough channel data of NITR (NITR3) as given in Table 2.

The present models have been verified through the data sets of large channel facility of FCF, data of Tominaga et al. (1989) and rough channel data of NITR (NITR3). The error in terms of MAPE for these three channels has been found to be 5%, 5.62%, and 3.78%, respectively, and for SKM model these values are found 8.16%, 5.75% and 4.45%, respectively. The average RMSE values for channels are found to be 0.055, 0.05 and 0.011, and for SKM these values are 0.08, 0.05 and 0.012, respectively, showing the strength of the model.

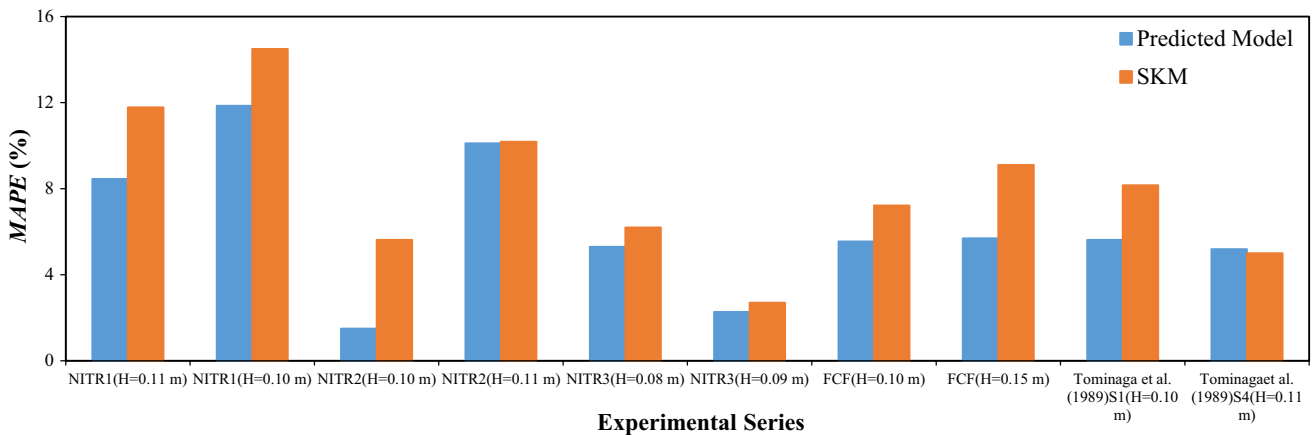


**Fig. 15** MAPE results of depth-averaged velocity distribution by different models

**Table 3** Geometric properties and surface conditions used for natural river data

Geometrical properties	River Senggi (B)	River Senggai
Bank full depth, $H(m)$	1.306	1.068
Top width, $T(m)$	5.285	5.5
Bed slope ( $S_0$ )	0.001	0.001
Surface condition (main channel)	Erodible Soil	Erodible Soil
Surface condition (side bank)	Long Vegetation	Erodible Soil
Manning's $n$ (main channel)	0.082	0.082
Manning's $n$ (side bank)	0.25	0.082

A reasonable error has been observed when the observed experimental results compared with SKM results and present model results for simple open channels with both smooth and rough case. The Shiono and Knight method (SKM) has shown satisfactory results for the prediction of depth-averaged velocity distribution in the lateral direction for both rectangular and trapezoidal channels. The philosophy of the SKM is based on using three calibrating coefficients for each

panel. But the present model is showing better results than SKM as proved from the results of MAPE and RMSE.

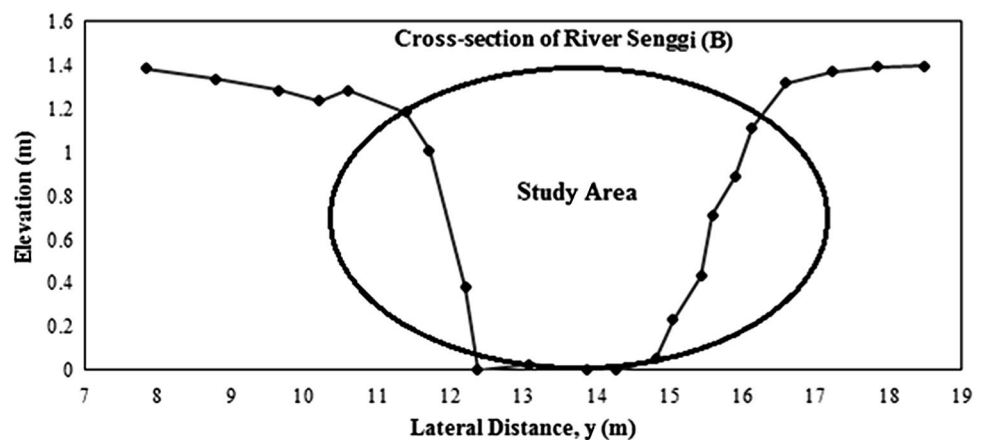
### Application of model to natural river

A new model is examined as efficient if it can predict accurately for field data. Applications of this model to two natural river data sets namely Senggi (B) and Senggai are presented in this section. These two rivers located in Kuching, the capital city of Sarawak state, Malaysia. The morphological cross sections of these rivers are presented in Fig. 15. These rivers are almost straight and uniform in cross section. But the configurations of natural rivers are generally unsymmetrical and having uneven surface compared to laboratory channels. So, it is very rigorous task to validate the developed model with any natural river. For analysis, the geometrical perimeter and hydraulic area of the rivers have been changed to an accessible shape that the original perimeter and original area of cross sections remain same. The geometric, hydraulic and surface properties of natural river datasets are mentioned in Table 3.



**Fig. 16** Morphological cross section of river Senggi (B) and river Senggai (Hin et al. 2008)

**Fig. 17** Actual cross section of river Senggi (B)



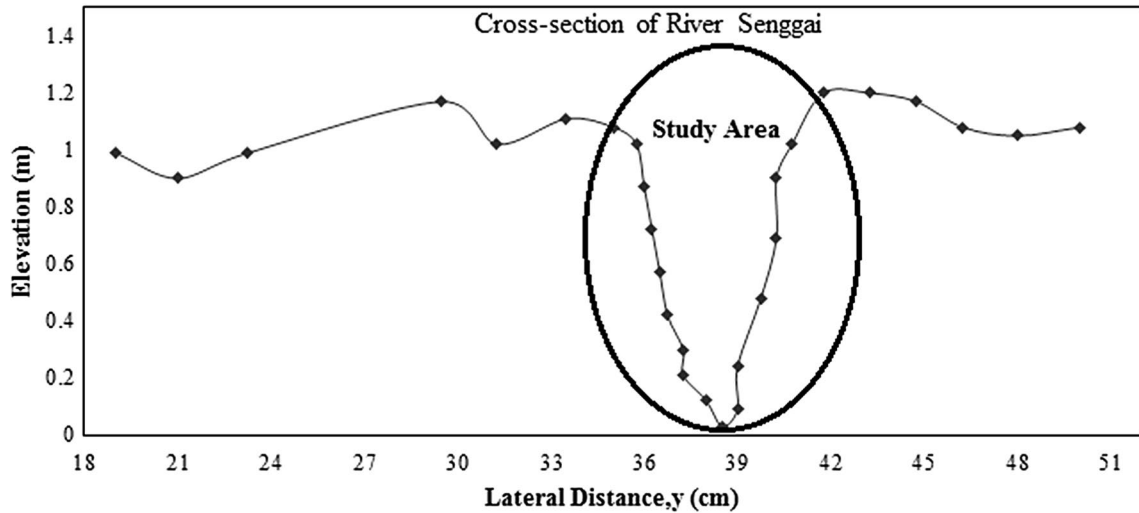


Fig. 18 Actual cross section of river Senggai

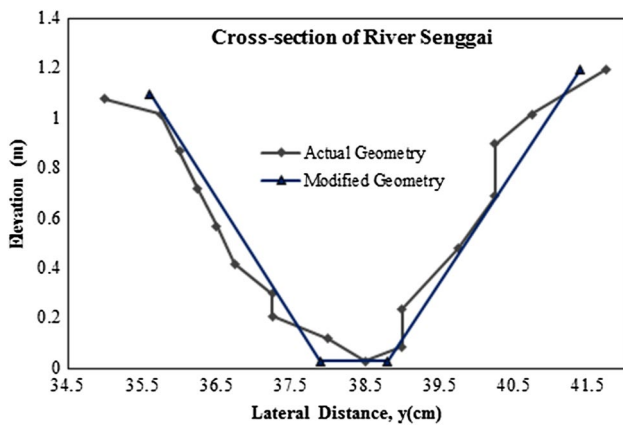


Fig. 19 Modified cross section of river Senggai equivalent to actual area

The actual cross-sectional geometry of river Senggai (B) is shown in Fig. 16. It is quite regular in cross-sectional geometry, so this can be accessible for validation. The observed depth-averaged velocity ( $U_d$ ) along the lateral cross section of river Senggai (B) for two in-bank flow depths ( $H=0.698$  m and 1.088 m) found from previous literature is considered for validation of the new approach. The value of lateral  $U_d$  resulted from present approach along with the values from SKM for these typical depths has been compared with field measurements. It is found that two methods approximately predict the  $U_d$  value nearer to observed values shown in Fig. 17.

The second river Senggai is irregular in its geometry mainly in the bed of the main channel. So it was quite

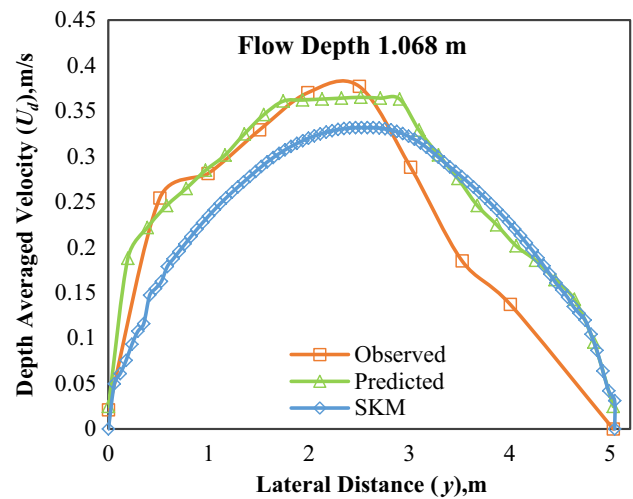
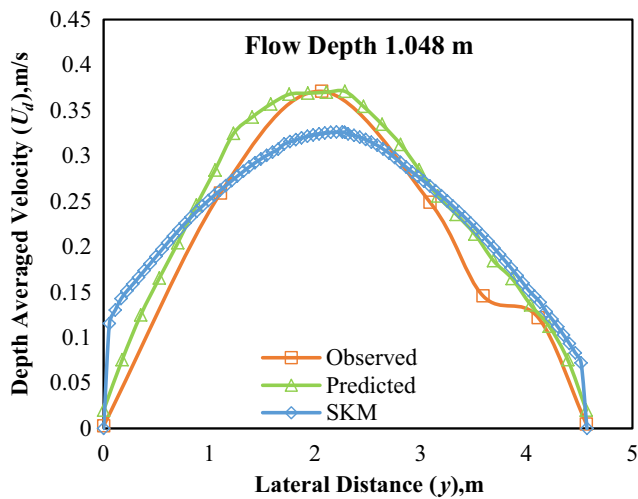


Fig. 20 Depth-averaged velocity of river Senggai

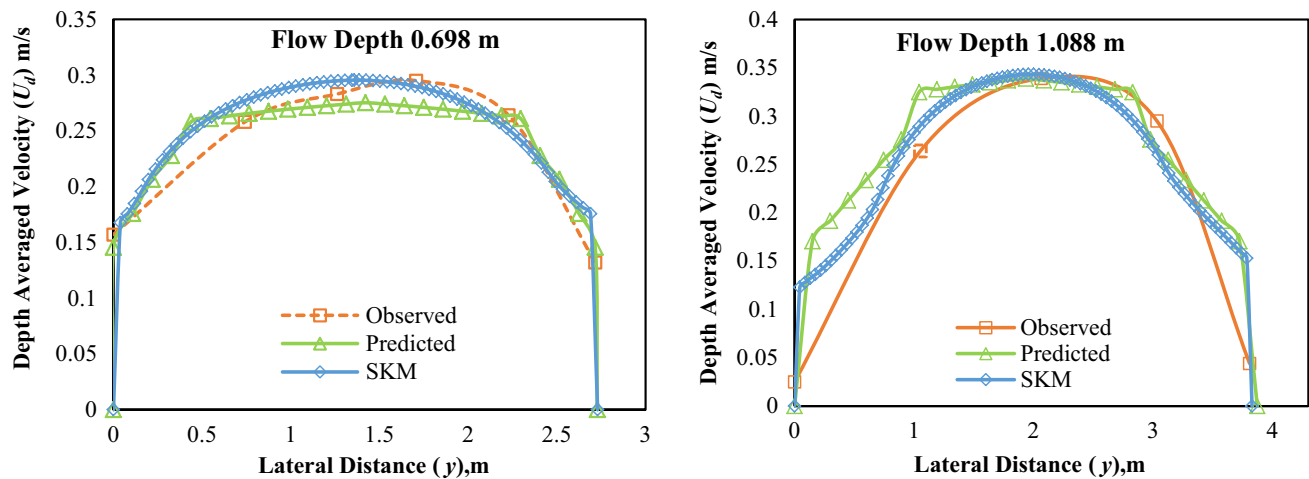


Fig. 21 Depth-averaged velocity of river Senggi (B)

difficult to take approximate depth from actual cross section of river Senggai as shown in Fig. 18 for comparing with predicted model and SKM. So, to overcome this difficulty a modified geometry has been considered keeping approximately the same perimeter and cross-sectional area as compared with the actual cross-sectional geometry as shown in Fig. 19. So the observed  $U_d$  value is uneven along the cross section. The observed depth-averaged velocity ( $U_d$ ) along the lateral cross section of river Senggai for two in-bank depths of flow ( $H = 1.048$  m and 1.068 m) found from previous literature is considered for validation of the new approach. The value of lateral  $U_d$  resulted from present approach over estimates the observed values and the SKM is found to under estimate the observed values shown in Fig. 20.

It has been found that the predicted  $U_d$  values are nearer to observed values with reasonable accuracy for both the natural river cases shown in Figs. 20 and 21, respectively.

## Conclusions

1. An experimental investigation has been carried out to find out the lateral depth-averaged velocity distribution for different flow depths of a smooth open channel flow.
2. The lateral velocity profiles at different horizontal planes are found to be power function, and vertical velocity profiles are found to be logarithmic in nature. Local velocity along the stream-wise direction for a given horizontal and vertical dimensions has been modelled.
3. The new expressions are found to be well matching with the observed values by providing less error.

The results of the predicted models have also been compared well with the popular Shiono and Knight Model (SKM). The SKM model is found to provide good velocity profile results; however, it fails to predict velocities at the junction between the constant flow depth domain and variable flow depth domain as occurred in trapezoidal cases.

4. The present models which are based on multi-variable regression analysis are found to provide very good results of velocity profiles for different laboratory channels.
5. Present models have been verified through the data sets of large channel facility of FCF, data of Tominaga et al. (1989) and NITR3. The errors in terms of MAPE for these three channels have been found to be 5%, 5.62%, and 3.78%, respectively. The MAPE values for SKM model are found 8.16%, 5.75%, and 4.45%, respectively, for these channels. The average RMSE values for these three channels are found to be 0.055, 0.05 and 0.011 and for SKM these values are 0.08, 0.05 and 0.012. So, the model is believed to predict the local velocity as well as the depth-averaged velocity for a channel with homogeneous roughness.
6. The predicted model has also been well validated against natural river datasets of river Senggi B and river Senggai with reasonable accuracy.

**Open Access** This article is distributed under the terms of the Creative Commons Attribution 4.0 International License (<http://creativecommons.org/licenses/by/4.0/>), which permits unrestricted use, distribution, and reproduction in any medium, provided you give appropriate credit to the original author(s) and the source, provide a link to the Creative Commons license, and indicate if changes were made.



## References

- Ansari K, Morvan HP, Hargreaves DM (2011) Numerical investigation into secondary currents and wall shear in trapezoidal channels. *J Hydraul Eng* 137(4):432–440
- Blumberg AF, Galperin B, O'Connor DJ (1992) Modeling vertical structure of open-channel flows. *J Hydraul Eng* 118(8):1119–1134
- De Cacqueray N, Hargreaves DM, Morvan HP (2009) A computational study of shear stress in smooth rectangular channels. *J Hydraul Res* 47(1):50–57
- Devi K, Khatua KK (2016) Prediction of depth averaged velocity and boundary shear distribution of a compound channel based on the mixing layer theory. *Flow Meas Instrum* 50:147–157
- Hin LS, Bessaih N, Ling LP, Ghani AA, Zakaria NA, Seng MY (2008) Discharge estimation for equatorial natural rivers with overbank flow. *Int J River Basin Manag* 6(1):13–21
- Jan CD, Chang CJ, Kuo FH (2009) Experiments on discharge equations of compound broad-crested weirs. *J Irrig Drain Eng* 135(4):511–515
- Jesson M, Sterling M, Bridgeman J (2012) Modeling flow in an open channel with heterogeneous bed roughness. *J Hydraul Eng* 139(2):195–204
- Khuntia JR, Devi K, Khatua KK (2016) Variation of local friction factor in an open channel flow. *Indian J Sci Technol* 9(46):1–6
- Liao H, Knight DW (2007) Analytic stage-discharge formulas for flow in straight prismatic channels. *J Hydraul Eng* 133(10):1111–1122
- Maghrebi MF, Givehchi M (2009) Estimation of depth-averaged velocity and boundary shear stress in a triangular open channel. *J Water Wastewater* 2:71–80
- Nezu I, Kadota A, Nakagawa H (1997) Turbulent structure in unsteady depth-varying open-channel flows. *J Hydraul Eng* 123(9):752–763
- Sarma KV, Lakshminarayana P, Rao NL (1983) Velocity distribution in smooth rectangular open channels. *J Hydraul Eng* 109(2):270–289
- Shiono K, Feng T (2003) Turbulence measurements of dye concentration and effects of secondary flow on distribution in open channel flows. *J Hydraul Eng* 129(5):373–384
- Shiono K, Knight DW (1990) Mathematical models of flow in two or multi stage straight channels. In: *Proceedings of the international conference on river flood hydraulics*. Wiley, New York, pp 229–238
- Steffler PM, Rajaratnam N, Peterson AW (1985) LDA measurements in open channel. *J Hydraul Eng* 111(1):119–130
- Tominaga A, Nezu I, Ezaki K, Nakagawa H (1989) Three-dimensional turbulent structure in straight open channel flows. *J Hydraul Res* 27(1):149–173
- Yang K, Nie R, Liu X, Cao S (2012) Modeling depth-averaged velocity and boundary shear stress in rectangular compound channels with secondary flows. *J Hydraul Eng* 139(1):76–83
- Zarrati AR, Jin YC, Karimpour S (2008) Semianalytical model for shear stress distribution in simple and compound open channels. *J Hydraul Eng* 134(2):205–215

**Publisher's Note** Springer Nature remains neutral with regard to jurisdictional claims in published maps and institutional affiliations.